

Theory of Photon-Assisted Magnetoacoustic Resonance as a New Probe of Quadrupole Dynamics

Mikito Koga¹ and Masashige Matsumoto²

¹*Department of Physics, Faculty of Education, Shizuoka University, Shizuoka 422–8529, Japan*

²*Department of Physics, Faculty of Science, Shizuoka University, Shizuoka 422–8529, Japan*

Motivated by the recent progress of phonon-mediated control in quantum spin devices, we propose a possibility of hybrid measurement using electron paramagnetic resonance (EPR) and a surface acoustic wave (SAW). Considering quadrupole-strain (QS) couplings suggested for silicon vacancies, we present a minimum model of the two-level system to investigate a magnetoacoustic resonance (MAR) coupled to various strain modes driven by the SAW. The longitudinal and transverse QS couplings can be changed by rotating a magnetic field, which depends on a combination of the strain modes. Using the Floquet theory, we elucidate each coupling effect on the time-averaged transition probability, especially focus on a single-phonon transition process. The important result is that the longitudinal QS coupling brings about a sharp photon-assisted resonance and leads to an abrupt change in the field-angle dependent transition probability. Since this phonon transition process is always accompanied by the photon transition, the field angle for the sharp resonance peak can be detected by the EPR measurement. The hybrid EPR-MAR measurement is useful to confirm the existence of quadrupole degrees of freedom strongly coupled to elastic strains, and thus it is expected to be a complementary probe for the precise evaluation of quadrupole properties.

1. Introduction

Quadrupole degrees of freedom are important factors as well as spin degrees of freedom for high spin states possessing degenerate orbitals. A possibility of electromechanical control of nuclear spins has been reported by the recent experiment of a GaAs-based resonator.¹⁾ The emergence of sideband nuclear magnetic resonance peaks can be explained by the effect of dynamical quadrupole-strain (QS) coupling on the nuclear spin state. There is also a proposal of mechanically and electrically driven electron spin resonance for nitrogen-vacancy (NV) centers in diamond.²⁾ Experimentally, for the NV centers, phonon induced orbital transitions were detected by photoluminescence excitation spectroscopy.^{3–5)} Motivated by such progress of phonon-mediated control in spintronics, we theoretically investigate a possibility of hybrid measurement using electron paramagnetic resonance (EPR) and a surface acoustic wave (SAW).⁶⁾ For solid-state electrons, the dynamical QS coupling can be driven by the SAW. By combination of photon and phonon transition processes, more precise analysis is expected to identify the symmetries of quadrupoles and also to reveal hidden quadrupole properties. We propose that the photon-assisted magnetoacoustic resonance (MAR) can be adopted as a complementary or an alternative probe to the conventional measurements of quadrupole such as elastic softening, nuclear quadrupole resonance, resonant x-ray diffraction, and polarized neutron diffraction.⁷⁾

In particular, we can apply the idea of the hybrid EPR-MAR measurement to confirm an extremely strong strain coupling with a quadrupole moment that possibly emerges in a silicon vacancy. This surprisingly strong QS coupling was first reported by bulk measurements of elastic softening in a boron-doped silicon wafer.^{8–11)} The significance of an orbitally degenerate vacancy state was also suggested by early theoretical studies.^{12–14)} The precise evaluation of vacancy concentration in the surface of a silicon wafer is inevitably required for information technology of semiconductor devices.

In the SAW measurement for the silicon vacancy, the elastic strains are driven by oscillating strain modes such as selected quadrupole symmetries $2z^2 - x^2 - y^2$, $x^2 - y^2$, and zx for the SAW propagating in the x direction of the crystal axis.¹¹⁾ Owing to the magnetic-field-dependent multiplet, each QS coupling can be changed by rotating an applied magnetic field and can be evaluated by probing a coupled photon-phonon transition in the EPR measurement.

The Floquet theory is very powerful for examining the two-level system that interacts with a periodically oscillating field. In the Floquet formalism, a problem of solving a time-dependent Schrödinger equation is transformed to a time-independent eigenvalue problem based on an infinite-dimensional matrix form of the Floquet Hamiltonian.^{15–19)} In the present study, there are both diagonal (longitudinal) and off-diagonal (transverse) couplings with the oscillating field related to various phonon modes. It is the most important to elucidate the former coupling effect on the photon-assisted transition in a single-phonon resonance process. The significance of the longitudinal coupling effect was previously studied in a different context of a superconducting quantum interference device driven by an ac field.^{16,17)} The key points are the energy shift of a sharp resonance peak and the peak broadening. Considering the transverse coupling effect as well, we extend the Floquet theory, which was frequently applied to multiphoton resonance processes in quantum devices,²⁰⁾ to investigate a more complicated problem of phonon-mediated transition processes in solid-state electronic spin systems.

This paper is organized as follows. In the first part of Sect. 2, we present a minimum model for the two-level system including QS couplings and derive this model from a realistic system suggested for the silicon vacancy. We compute the longitudinal and transverse QS couplings with the strain modes, which are given as a function of the rotation angle of the magnetic field. In the second part, the Floquet Hamiltonian is derived for the two-level system coupled to the SAW phonons.

For nearly degenerate Floquet states, it is useful to analyze an effective 2×2 matrix formulated by the Van Vleck perturbation theory for a multi-phonon resonance.^{16,17} In Sect. 3, we elucidate the longitudinal-mode and transverse-mode coupling effects on the time-averaged transition probability. Next, we show the field-angle dependence of the transition probability and how to evaluate the QS couplings with different symmetries. Finally, the conclusion and discussion are given by Sect. 4.

2. Model

2.1 Quadrupole-strain couplings in two-level system

To extract essential roles of QS couplings in the transition probabilities detected by the EPR, we study a minimum model of the two-level system described by the following Hamiltonian $H = H_0 + H_{\text{QS}} + H_{\text{MW}}$:⁵

$$H_0 = \frac{1}{2}\hbar\omega_0(-|g\rangle\langle g| + |e\rangle\langle e|), \quad (1)$$

$$H_{\text{QS}} = \frac{1}{2}g_L\varepsilon_L(t)(|g\rangle\langle g| - |e\rangle\langle e|) + \frac{1}{2}g_T\varepsilon_T(t)(|g\rangle\langle e| + |e\rangle\langle g|), \quad (2)$$

$$H_{\text{MW}} = \frac{1}{2}\hbar\Omega(|g\rangle\langle e|e^{i\omega_l t} + |e\rangle\langle g|e^{-i\omega_l t}), \quad (3)$$

where $|g\rangle$ and $|e\rangle$ represent the wave functions of the ground and excited states of the two-level system, respectively, with the energy difference $\hbar\omega_0$. In Eq. (2), g_L (g_T) is a QS coupling constant for the longitudinal (transverse) vibration modes between the two states, and the displacement ε_L (ε_T) with the time t dependence represents an elastic strain of the acoustic-wave L -mode (T -mode) coupled to quadrupoles. Equation (3) describes the absorption ($|e\rangle\langle g|$) and emission ($|g\rangle\langle e|$) processes of a microwave (MW) with frequency ω_l , and the Rabi frequency Ω characterizes the periodic oscillation of the time-dependent transition probability. Here, the rotating wave approximation (RWA) has been considered.⁵ In the conventional manner, we introduce a unitary transformation $U = e^{-i\omega_l t I_z}$, where the pseudospin operator I is defined by

$$I_z = \frac{1}{2}(|g\rangle\langle g| - |e\rangle\langle e|), \quad (4)$$

$$I_x = \frac{1}{2}(|g\rangle\langle e| + |e\rangle\langle g|) \equiv \frac{1}{2}(I_+ + I_-), \quad (5)$$

and $I_y = i[I_z, I_x]$. Transforming the original Hamiltonian H into the rotating frame, we have

$$\begin{aligned} \tilde{H} &= UH U^\dagger - i\hbar U \frac{\partial U^\dagger}{\partial t} \\ &= -[\hbar(\omega_0 - \omega_l) + g_L\varepsilon_L(t)]I_z \\ &\quad + \frac{1}{2}g_T\varepsilon_T(t)(I_+ e^{-i\omega_l t} + I_- e^{i\omega_l t}) + \hbar\Omega I_x. \end{aligned} \quad (6)$$

This means that the original Schrödinger equation is transformed as

$$i\hbar \frac{\partial}{\partial t} |\psi\rangle = H |\psi\rangle \rightarrow i\hbar \frac{\partial}{\partial t} U |\psi\rangle = \tilde{H} U |\psi\rangle. \quad (7)$$

For the propagating SAW, the elastic strain components are given by

$$\varepsilon_L(t) = a_L \cos(\omega_m t + \phi_L), \quad \varepsilon_T(t) = a_T \cos(\omega_m t + \phi_T), \quad (8)$$

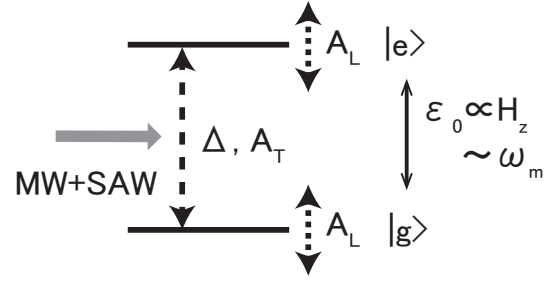


Fig. 1. Two-level system ($|g\rangle$ and $|e\rangle$) coupled to strain modes driven by the SAW. The transition between $|g\rangle$ and $|e\rangle$ occurs through the transverse QS coupling (A_T) in addition to the MW photon coupling (Δ). The transition is also due to the longitudinal QS coupling (A_L) in a photon-assisted transition process. Here, the detuning energy ε_0 is almost proportional to the magnetic field H_z for the Zeeman splitting comparable to the single-phonon energy $\hbar\omega_m$.

where ω_m is the SAW frequency, a_L (a_T) is the amplitude of the L -mode (T -mode), and the phase shift ϕ_L (ϕ_T) depends on the positions in the direction of the propagating SAW. Notice that the phase difference $\phi_T - \phi_L$ is constant. Keeping in mind an ultrasonic measurement of gigahertz order, we assume $\omega_m \gg \omega_l$ ($\omega_m \pm \omega_l \approx \omega_m$) in the following discussion. For the high frequency SAW, the transformed Hamiltonian \tilde{H} is reduced to

$$\begin{aligned} \tilde{H}(t) &= -[\varepsilon_0 + \frac{1}{2}(A_L e^{i\omega_m t} + A_L^* e^{-i\omega_m t})]I_z \\ &\quad + \frac{1}{2}(A_T e^{i\omega_m t} + A_T^* e^{-i\omega_m t})I_x \\ &\quad + \frac{1}{2}(\Delta^* I_+ + \Delta I_-), \end{aligned} \quad (9)$$

where

$$\varepsilon_0 = \hbar(\omega_0 - \omega_l), \quad A_L = -g_L a_L e^{i\phi_L}, \quad A_T = g_T a_T e^{i\phi_T}. \quad (10)$$

In the last term of $\tilde{H}(t)$, we consider a relative phase difference of the coupled photon and phonon as $\Delta = |\Delta|e^{i\phi_l} = \hbar\Omega e^{i\phi_l}$, and ϕ_l may take arbitrary values owing to random distributions of local quadrupoles (vacancies) in a crystal. For $|\Delta|/\hbar\omega_m \ll 1$, the calculated transition probability is not much dependent on ϕ_l as discussed later. Each term in Eq. (9) is sketched by Fig. 1. For understanding the present two-level system, it is helpful to express a matrix form of $\tilde{H}(t)$ on the basis of $\{|g\rangle, |e\rangle\}$ as

$$\tilde{H}(t) = \frac{1}{2} \begin{pmatrix} -\varepsilon_0 & \Delta^* \\ \Delta & \varepsilon_0 \end{pmatrix} + \frac{1}{2} \begin{pmatrix} -A_L(\omega_m t) & A_T(\omega_m t) \\ A_T(\omega_m t) & A_L(\omega_m t) \end{pmatrix}, \quad (11)$$

and $A_{L(T)}(\omega_m t) = (A_{L(T)} e^{i\omega_m t} + A_{L(T)}^* e^{-i\omega_m t})/2$. For $\Delta = 0$, the time-dependent diagonal coupling with A_L only changes the energy difference $\varepsilon_0 = \hbar\omega_0$ and does not contribute to the direct transition between $|g\rangle$ and $|e\rangle$. However, this coupling plays an important role in a photon-assisted transition process for a finite Δ .

2.2 Derivation of two-level system in a realistic case

Here, considering the quartet ground state proposed for the silicon vacancy, we describe the QS interaction with elastic strains driven by the SAW. A combination of QS couplings with different symmetries is changed by rotating an applied

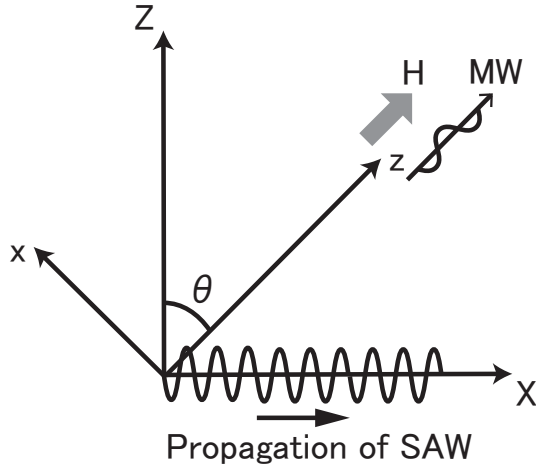


Fig. 2. Schematic diagram of hybrid measurement with EPR and SAW. The (X, Z) and (x, z) coordinates are set for the SAW propagating along the X axis and for the rotating static magnetic field H parallel to the z axis, respectively. The MW magnetic field oscillates along the x axis. For a silicon wafer, vacancies are distributed randomly in the XY plane of the surface layer.

magnetic field. We derive the two-level system for the ground and first excited states lifted from the degenerate quartet in the magnetic field. The derivation presented here is also applicable to other quartet systems as well as the silicon vacancy.

In the boron-doped silicon wafer, the elastic softening is well explained by the strong QS coupling with the vacancy orbital.^{9,10} It is expected that the electronic state with orbital $L = 1$ and spin $S = 1/2$ forms the Γ_8 quartet ground and Γ_7 doublet excited states, owing to the spin-orbit interaction in the T_d cubic crystal-field environment. We restrict ourselves to the Γ_8 quartet described by the $J = 3/2$ angular momentum operator. As illustrated in Fig. 2, we consider that the SAW propagates in the $X||[100]$ direction on the $Z||[001]$ surface of the silicon wafer in the presence of an external magnetic field rotating around $Y||[010]$ in the ZX plane. Under this experimental setting, the elastic strains coupled to the quadrupoles are given by the following three components:¹¹⁾

$$\varepsilon_U = \frac{1}{\sqrt{3}}(2\varepsilon_{ZZ} - \varepsilon_{XX} - \varepsilon_{YY}), \quad (12)$$

$$\varepsilon_V = \varepsilon_{XX} - \varepsilon_{YY}, \quad (13)$$

$$\varepsilon_{ZX} = \frac{\partial u_X}{\partial Z} + \frac{\partial u_Z}{\partial X}, \quad (14)$$

where u_i ($i = X, Y, Z$) is a displacement vector component and $\varepsilon_{ii} = \partial u_i / \partial x_i$ ($x_i = i = X, Y, Z$). Here, an irrelevant u_Y has been considered for the SAW propagating along the X axis, and $\varepsilon_{YZ} = \varepsilon_{XY} = 0$.¹¹⁾ As a consequence, the interaction of the Γ_8 quadrupoles and local strains in the magnetic field can be described by $H_{\text{local}} = H_{\text{Zeeman}} + H_{\text{QS}}$:

$$H_{\text{Zeeman}} = -g_J \mu_B \mathbf{J} \cdot \mathbf{H}, \quad (15)$$

$$H_{\text{QS}} = g_{\Gamma_3}(O_U \varepsilon_U + O_V \varepsilon_V) + g_{\Gamma_5} O_{ZX} \varepsilon_{ZX}. \quad (16)$$

Here, the quadrupole operators are represented by the second-rank tensor operators of $\mathbf{J} = (J_X, J_Y, J_Z)$ as

$$O_U = \frac{1}{\sqrt{3}}(2J_Z^2 - J_X^2 - J_Y^2), \quad (17)$$

$$O_V = J_X^2 - J_Y^2, \quad (18)$$

$$O_{ZX} = J_Z J_X + J_X J_Z. \quad (19)$$

In Eq. (15) of the Zeeman term, g_J is the Landé's g factor and μ_B is the Bohr magneton. Equation (16) consists of the Γ_3 and Γ_5 irreducible representations in the cubic point group with the QS coupling constants g_{Γ_3} and g_{Γ_5} , respectively.

Next, we consider the rotation of the magnetic field and choose the z axis parallel to $\mathbf{H}/|\mathbf{H}| = (\sin \theta, 0, \cos \theta)$ in the ZX plane. Accordingly, the x and y axes are set as $x||(-\cos \theta, 0, \sin \theta)$ and $y||(0, -1, 0)$. The components of the \mathbf{J} operator in the (xyz) coordinate are related to those in the (XYZ) crystal coordinate as

$$\begin{cases} J_x = -\cos \theta \cdot J_X + \sin \theta \cdot J_Z, \\ J_y = -J_Y, \\ J_z = \sin \theta \cdot J_X + \cos \theta \cdot J_Z. \end{cases} \quad (20)$$

Under the field parallel to the z axis, it is convenient to replace the quadrupole operators in Eqs. (17)–(19) by the linear combination of $O_u = (2J_z^2 - J_x^2 - J_y^2)/\sqrt{3}$, $O_v = J_x^2 - J_y^2$, and $O_{zx} = J_z J_x + J_x J_z$:

$$\begin{cases} O_U \rightarrow -\frac{1-3\cos^2\theta}{2}O_u + \frac{\sqrt{3}}{2}\sin^2\theta \cdot O_v \\ \quad + \sqrt{3}\sin\theta\cos\theta \cdot O_{zx}, \\ O_V \rightarrow \frac{\sqrt{3}}{2}\sin^2\theta \cdot O_u + \frac{1+\cos^2\theta}{2}O_v - \sin\theta\cos\theta \cdot O_{zx}, \\ O_{ZX} \rightarrow \sqrt{3}\sin\theta\cos\theta \cdot O_u - \sin\theta\cos\theta \cdot O_v - \cos 2\theta \cdot O_{zx}. \end{cases} \quad (21)$$

On the basis of the eigenstates of J_z ($= \pm 1/2, \pm 3/2$), the field-angle dependence of the QS interaction in Eq. (16) is explicitly written as $H_{\text{QS}} = A_u O_u + A_v O_v + A_{zx} O_{zx}$, where

$$\begin{aligned} A_u = g_{\Gamma_3} & \left[\left(\frac{1}{4}\varepsilon_U + \frac{\sqrt{3}}{4}\varepsilon_V \right) + \left(\frac{3}{4}\varepsilon_U - \frac{\sqrt{3}}{4}\varepsilon_V \right) \cos 2\theta \right] \\ & + g_{\Gamma_5} \left(\frac{\sqrt{3}}{2}\varepsilon_{ZX} \right) \sin 2\theta, \end{aligned} \quad (22)$$

$$\begin{aligned} A_v = g_{\Gamma_3} & \left[\left(\frac{\sqrt{3}}{4}\varepsilon_U + \frac{3}{4}\varepsilon_V \right) + \left(-\frac{\sqrt{3}}{4}\varepsilon_U + \frac{1}{4}\varepsilon_V \right) \cos 2\theta \right] \\ & + g_{\Gamma_5} \left(-\frac{1}{2}\varepsilon_{ZX} \right) \sin 2\theta, \end{aligned} \quad (23)$$

$$A_{zx} = g_{\Gamma_3} \left(\frac{\sqrt{3}}{2}\varepsilon_U - \frac{1}{2}\varepsilon_V \right) \sin 2\theta + g_{\Gamma_5} (-\varepsilon_{ZX}) \cos 2\theta. \quad (24)$$

For a strong magnetic field $g_J \mu_B H_z \sim \hbar \omega_m$, we focus on the quadrupole-stain coupling between the ground state with $J_z = 3/2$ denoted by $|g\rangle$ and the first excited state with $J_z = 1/2$ denoted by $|e\rangle$ for H_{Zeeman} . In the subspace of the two states, $\hbar \omega_0 = g_J \mu_B H_z$ in Eq. (10), and the quadrupole operators O_u and O_{zx} are reduced to

$$O_u = \sqrt{3}(|g\rangle\langle g| - |e\rangle\langle e|) = 2\sqrt{3}I_z, \quad (25)$$

$$O_{zx} = \sqrt{3}(|g\rangle\langle e| + |e\rangle\langle g|) = 2\sqrt{3}I_x, \quad (26)$$

and there is no O_v coupling between $|g\rangle$ and $|e\rangle$. For the local strain components of the propagating SAW,

$$\varepsilon_i(t) = a_i \cos(\omega_m t + \phi_i) \quad (27)$$

represents one of the three strain modes ($i = U, V, ZX$), where

a_i is the local amplitude of each mode and the phase shift ϕ_i is given as $(-kX + \phi_{i,0})$ in the X direction of the SAW with wave number k ($= \omega_m/v$; v is the sound velocity) and initial phase shift $\phi_{i,0}$. Notice that the phase differences $\phi_i - \phi_j$ ($i, j = U, V, ZX$) are constant. Since $A_{\mu}O_{\mu}$ and $A_{zx}O_{zx}$ correspond to the L -mode and T -mode in Eq. (9), respectively, we obtain

$$H_{QS} = g_L a_L \cos(\omega_m t + \phi_L) I_z + g_T a_T \cos(\omega_m t + \phi_T) I_x, \quad (28)$$

where $g_{\mu} a_{\mu}$ ($\mu = L, T$) are determined from

$$g_{\mu} a_{\mu} \begin{pmatrix} \cos \phi_{\mu} \\ \sin \phi_{\mu} \end{pmatrix} = C_{\mu,0} + C_{\mu,1} \cos 2\theta + C_{\mu,2} \sin 2\theta. \quad (29)$$

The coefficients $C_{\mu,i}$ ($i = 0, 1, 2$) depend on a_i and ϕ_i in Eq. (27) as

$$C_{L,0} = \sqrt{3} g_{\Gamma_3} \left[\frac{1}{2} a_U \begin{pmatrix} \cos \phi_U \\ \sin \phi_U \end{pmatrix} + \frac{\sqrt{3}}{2} a_V \begin{pmatrix} \cos \phi_V \\ \sin \phi_V \end{pmatrix} \right], \quad (30)$$

$$C_{L,1} = 3 g_{\Gamma_3} \left[\frac{\sqrt{3}}{2} a_U \begin{pmatrix} \cos \phi_U \\ \sin \phi_U \end{pmatrix} - \frac{1}{2} a_V \begin{pmatrix} \cos \phi_V \\ \sin \phi_V \end{pmatrix} \right], \quad (31)$$

$$C_{L,2} = 3 g_{\Gamma_5} a_{ZX} \begin{pmatrix} \cos \phi_{ZX} \\ \sin \phi_{ZX} \end{pmatrix}, \quad (32)$$

$$C_{T,1} = -2 \sqrt{3} g_{\Gamma_5} a_{ZX} \begin{pmatrix} \cos \phi_{ZX} \\ \sin \phi_{ZX} \end{pmatrix}, \quad (33)$$

$$C_{T,2} = 2 \sqrt{3} g_{\Gamma_3} \left[\frac{\sqrt{3}}{2} a_U \begin{pmatrix} \cos \phi_U \\ \sin \phi_U \end{pmatrix} - \frac{1}{2} a_V \begin{pmatrix} \cos \phi_V \\ \sin \phi_V \end{pmatrix} \right], \quad (34)$$

and $C_{T,0}$ vanishes.

2.3 Floquet Hamiltonian

According to the Floquet theory,¹⁵⁾ the time-dependent Schrödinger equation

$$i\hbar \frac{\partial \psi(t)}{\partial t} = H(t) \psi(t), \quad (35)$$

where $H(t)$ is periodic in time, is solved by the following eigenvalue equation

$$\left[H(t) - i\hbar \frac{\partial}{\partial t} \right] \phi(t) = q \phi(t). \quad (36)$$

The time-periodic wave function $\phi(t)$ is related to $\psi(t)$ as $\psi(t) = e^{-iqt/\hbar} \phi(t)$ with the quasienergy q . The periodic time-dependent differential equation is transformed to a time-independent infinite-dimensional matrix eigenvalue problem through the Fourier expansion

$$H(t) = \sum_{n=-\infty}^{\infty} H^{[n]} e^{in\omega t}, \quad \phi(t) = \sum_{n=-\infty}^{\infty} \phi^{[n]} e^{in\omega t}, \quad (37)$$

and Eq. (36) is reduced to

$$\sum_m [H^{[n-m]} + n\hbar\omega\delta_{nm}] \phi^{[m]} = q \phi^{[n]}, \quad (38)$$

where δ_{nm} is the Kronecker delta. Let us introduce a trial eigenstate $|q_{\gamma}\rangle$ with the corresponding eigenvalue q_{γ} , which satisfies

$$\sum_m [H^{[n-m]} + n\hbar\omega\delta_{nm}] |q_{\gamma}\rangle = q_{\gamma} |q_{\gamma}\rangle, \quad (39)$$

and the integers m and n run from $-\infty$ to ∞ . Using orthogonal states labeled by α and β in the two-level system, Eq. (38) is rewritten as

$$\sum_m \sum_{\beta} \langle \alpha n | H_F | \beta m \rangle \langle \beta m | q_{\gamma} \rangle = q_{\gamma} \langle \alpha n | q_{\gamma} \rangle. \quad (40)$$

Here, the eigenvector $\langle \alpha n | q_{\gamma} \rangle$ ($\equiv \phi_{\alpha\gamma}^{[n]}$) is represented by a Floquet state $|\alpha n\rangle = |\alpha\rangle \otimes |n\rangle$ which is considered as an oscillating-field dressed state ($|n\rangle$ is also related to $\langle t|n\rangle \equiv e^{in\omega t}$). The matrix expression of the Floquet Hamiltonian

$$\langle \alpha n | H_F | \beta m \rangle = H_{\alpha\beta}^{[n-m]} + n\hbar\omega\delta_{nm}\delta_{\alpha\beta} \quad (41)$$

is constructed by an infinite number of $|\alpha n\rangle$. Indeed, $H_F |q_{\gamma}\rangle = q_{\gamma} |q_{\gamma}\rangle$ in Eq. (40) is extended to the generalized eigenvalue problem $H_F |q_{\gamma l}\rangle = q_{\gamma l} |q_{\gamma l}\rangle$, where $q_{\gamma l} = q_{\gamma} + l\hbar\omega$ and $\langle \alpha n | q_{\gamma l} \rangle = \langle \alpha, n-l | q_{\gamma} \rangle$ are satisfied.^{15,21)} Owing to this translational invariance, it is sufficient to solve the essential eigenvalue q_{γ} by diagonalizing H_F . In the following discussion, $\hbar = 1$ is used for simplicity.

Let us apply the above matrix expression of the Floquet Hamiltonian in Eq. (41) to the two-level system coupled to the SAW and the MW in Eq. (9), where the SAW phonon frequency ω_m is replaced by ω . First, the block Hamiltonian in the subspace of $\{|gn\rangle, |en\rangle\}$ for the same integer n can be written as

$$H_n^{[0]} \equiv H^{[0]} + n\omega = \begin{pmatrix} -(\varepsilon_0/2) + n\omega & \Delta^*/2 \\ \Delta/2 & (\varepsilon_0/2) + n\omega \end{pmatrix}. \quad (42)$$

There are only finite matrix elements between $|g$ (or e), n and $|g$ (or e), $m = n \pm 1$ in Eq. (41), and the corresponding block matrix parts are given by

$$H^{[1]} = \frac{1}{4} \begin{pmatrix} -A_L & A_T \\ A_T & A_L \end{pmatrix}, \quad H^{[-1]} = \frac{1}{4} \begin{pmatrix} -A_L^* & A_T^* \\ A_T^* & A_L^* \end{pmatrix}, \quad (43)$$

while $H^{[n]} = \mathbf{0}$ ($|n| \geq 2$), where all elements are zeros in the 2×2 matrix $\mathbf{0}$. Using these block matrices, the Floquet matrix is written as

$$H_F = \begin{pmatrix} \ddots & & & & & & & \vdots \\ & H_{-2}^{[0]} & H^{[-1]} & \mathbf{0} & \mathbf{0} & \mathbf{0} & & \\ & H^{[1]} & H_{-1}^{[0]} & H^{[-1]} & \mathbf{0} & \mathbf{0} & & \\ \cdots & \mathbf{0} & H^{[1]} & H_0^{[0]} & H^{[-1]} & \mathbf{0} & \cdots & \\ & \mathbf{0} & \mathbf{0} & H^{[1]} & H_1^{[0]} & H^{[-1]} & & \\ & \mathbf{0} & \mathbf{0} & \mathbf{0} & H^{[1]} & H_2^{[0]} & & \\ & & & & \vdots & & & \ddots \end{pmatrix}. \quad (44)$$

Eigenvalues and the corresponding eigenvectors are solved by a finite number of blocks of the Floquet matrix. As reported by Ref. 16, we choose $n \approx 50$, namely, from $H_{-50}^{[0]}$ to $H_{50}^{[0]}$ in Eq. (44), and check that the numerical results are sufficiently converged. Here, we devote ourselves to calculate the time-averaged transition probability between the two states $|g\rangle$ and $|e\rangle$,¹⁵⁾

$$\bar{P}_{g \rightarrow e} = \sum_m \sum_{\gamma} |\langle em | q_{\gamma} \rangle \langle q_{\gamma} | g0 \rangle|^2, \quad (45)$$

in the energy region $0 < \varepsilon_0 < 2\omega$, and focus on a single phonon process at around $\varepsilon_0 = \omega$.

Inclusion of T -mode phonons ($A_T \neq 0$) makes the numerical analysis more complicated than the case of $A_T = 0$ where

only L -mode phonons are coupled to photons. For the latter, sharp peaks of the transition probability are generated at around $\varepsilon_0 = \omega, 2\omega, \dots$ for a strong oscillating field of the L -mode $|A_L|/\omega \gg 1$. Owing to a finite amplitude A_T , these peaks become broad and the n th peak positions shift away from $\varepsilon_0 = n\omega$. It is also marked that the appearance of the transition probability peaks is affected by the phase difference $\theta_T - \theta_L$ between the two phonon modes as well as the amplitudes $|A_L|/\omega$ and $|A_T|/\omega$. In addition, for the photon-phonon coupled process, it is necessary to consider the phase shift ϕ_l of $\Delta = |\Delta|e^{i\phi_l}$ as well as the amplitude $|\Delta|$. As discussed in the previous subsection, A_μ ($\mu = L, T$) is related to the QS coupling amplitude $g_\mu a_\mu$ and the phase shift ϕ_μ of the μ -mode, which changes with the rotation angle θ of the magnetic field as shown in Eq. (29).

2.4 Nearly degenerate Floquet states

It is very useful to consider the nearly degenerate Floquet states which are involved in a multiphonon process, and this is formulated by the Van Vleck perturbation theory. The derivation of an effective Hamiltonian for the almost degenerate levels was reported in a similar case of the two-level system coupled to an oscillating field.^{16,17} We extend the previous formulation including a direct off-diagonal coupling of the oscillating field between the two states, namely, A_T of the T -mode phonons in addition to A_L of the L -mode phonons.

Let us start from an unperturbed Hamiltonian $H_{F,0} = H_F(\Delta = 0, A_T = 0)$ in Eq. (44), and the eigenvalue equations are given by

$$H_{F,0} |\tilde{g}n\rangle = \left(-\frac{\varepsilon_0}{2} + n\omega\right) |\tilde{g}n\rangle, \quad (46)$$

$$H_{F,0} |\tilde{e}m\rangle = \left(\frac{\varepsilon_0}{2} + m\omega\right) |\tilde{e}m\rangle. \quad (47)$$

Equation (46) corresponds to the following original differential equation

$$\left\{ \frac{1}{2} [-\varepsilon_0 - |A_L| \cos(\omega t + \theta_L)] - i \frac{\partial}{\partial t} \right\} \phi_n(t) = \lambda \phi_n(t), \quad (48)$$

where $A_L = |A_L|e^{i\theta_L}$ and $\lambda = -(\varepsilon_0/2) + n\omega$. The analytic solution is obtained as

$$\begin{aligned} \phi_n(t) &= e^{in\omega t} e^{i[|A_L|/(2\omega)] \sin(\omega t + \theta_L)} = \sum_{k=-\infty}^{\infty} e^{ik\theta_L} J_k \left(\frac{|A_L|}{2\omega} \right) e^{i(n+k)\omega t} \\ &= \sum_{k=-\infty}^{\infty} e^{i(k-n)\theta_L} J_{k-n} \left(\frac{|A_L|}{2\omega} \right) e^{ik\omega t}, \end{aligned} \quad (49)$$

which is expanded with the k th order Bessel functions $J_k(z)$. This leads to the expression of $|\tilde{g}n\rangle$ on the basis of the Floquet states $|gk\rangle$ as

$$|\tilde{g}n\rangle = \sum_{k=-\infty}^{\infty} e^{i(k-n)\theta_L} J_{k-n} \left(\frac{|A_L|}{2\omega} \right) |gk\rangle. \quad (50)$$

In the same manner for Eq. (47),

$$|\tilde{e}m\rangle = \sum_{k=-\infty}^{\infty} e^{i(k-m)\theta_L} J_{k-m} \left(-\frac{|A_L|}{2\omega} \right) |ek\rangle. \quad (51)$$

Next, for finite Δ and A_T , the Floquet matrix elements are rewritten on the new basis set of $\{|\tilde{g}n\rangle, |\tilde{e}m\rangle\}$ for any integer n and m . Using $J_n(2z) = \sum_m J_{n-m}(z) J_m(z)$ for $z = |A_L|/2\omega$, the

matrix element related to the transition $e \rightarrow g$ is calculated as

$$\begin{aligned} \langle \tilde{g}n | H_F | \tilde{e}m \rangle &= \sum_{k=-\infty}^{\infty} \sum_{l=-\infty}^{\infty} e^{-i(k-n)\theta_L} J_{k-n}(z) J_{l-m}(-z) \\ &\quad \times e^{i(l-m)\theta_L} \langle gk | H_F | el \rangle \\ &= \frac{\Delta^*}{2} \sum_{k=-\infty}^{\infty} e^{i(n-m)\theta_L} J_{k-n}(z) J_{-k+m}(z) \\ &\quad + \frac{|A_T|}{4} e^{i\theta_T} \sum_{k=-\infty}^{\infty} e^{i(n-m-1)\theta_L} J_{k-n}(z) J_{-k+m+1}(z) \\ &\quad + \frac{|A_T|}{4} e^{-i\theta_T} \sum_{k=-\infty}^{\infty} e^{i(n-m+1)\theta_L} J_{k-n}(z) J_{-k+m-1}(z) \\ &= e^{-i(m-n)\theta_L} \left[\frac{\Delta^*}{2} J_{m-n}(2z) + \frac{|A_T|}{4} e^{i(\theta_T - \theta_L)} J_{m-n+1}(2z) \right. \\ &\quad \left. + \frac{|A_T|}{4} e^{-i(\theta_T - \theta_L)} J_{m-n-1}(2z) \right] \equiv v_{m-n}^{\tilde{g}\tilde{e}}. \end{aligned} \quad (52)$$

In the same manner, $\langle \tilde{e}n | H_F | \tilde{g}m \rangle \equiv v_{n-m}^{\tilde{e}\tilde{g}} = (v_{n-m}^{\tilde{g}\tilde{e}})^*$ is obtained for the transition $g \rightarrow e$. For the matrix element related to the transition $g \rightarrow g$,

$$\begin{aligned} \langle \tilde{g}n | H_F | \tilde{g}m \rangle &= \sum_{k=-\infty}^{\infty} \sum_{l=-\infty}^{\infty} e^{-i(k-n)\theta_L} J_{k-n}(z) J_{l-m}(z) \\ &\quad \times e^{i(l-m)\theta_L} \langle gk | H_F | gl \rangle \\ &= \sum_{k=-\infty}^{\infty} e^{i(n-m)\theta_L} J_{k-n}(z) \left\{ \left(-\frac{\varepsilon_0}{2} + k\omega \right) J_{k-m}(z) \right. \\ &\quad \left. - \frac{|A_L|}{4} [J_{k-m-1}(z) + J_{k-m+1}(z)] \right\}. \end{aligned} \quad (53)$$

Using $J_{n-1}(z) + J_{n+1}(z) = 2nJ_n(z)/z$ and the summation $\sum_m J_m(z) J_{m-n}(z) = \delta_{n0}$, we obtain

$$\begin{aligned} \langle \tilde{g}n | H_F | \tilde{g}m \rangle &= e^{i(n-m)\theta_L} \left(-\frac{\varepsilon_0}{2} + m\omega \right) \sum_{k=-\infty}^{\infty} J_{k-n}(z) J_{k-m}(z) \\ &= \left(-\frac{\varepsilon_0}{2} + n\omega \right) \delta_{nm}. \end{aligned} \quad (54)$$

In the same manner, for the transition $e \rightarrow e$,

$$\langle \tilde{e}n | H_F | \tilde{e}m \rangle = \left(\frac{\varepsilon_0}{2} + n\omega \right) \delta_{nm}. \quad (55)$$

In the above calculations, the following matrix elements have been used:

$$\langle gk | H_F | el \rangle = \frac{\Delta^*}{2} \delta_{kl} + \frac{|A_T|}{4} (e^{i\theta_T} \delta_{k,l+1} + e^{-i\theta_T} \delta_{k,l-1}), \quad (56)$$

$$\langle ek | H_F | gl \rangle = \frac{\Delta}{2} \delta_{kl} + \frac{|A_T|}{4} (e^{i\theta_T} \delta_{k,l+1} + e^{-i\theta_T} \delta_{k,l-1}), \quad (57)$$

$$\langle gk | H_F | gl \rangle = \left(-\frac{\varepsilon_0}{2} + k\omega \right) \delta_{kl} - \frac{|A_L|}{4} (e^{i\theta_L} \delta_{k,l+1} + e^{-i\theta_L} \delta_{k,l-1}), \quad (58)$$

$$\langle ek | H_F | el \rangle = \left(\frac{\varepsilon_0}{2} + k\omega \right) \delta_{kl} + \frac{|A_L|}{4} (e^{i\theta_L} \delta_{k,l+1} + e^{-i\theta_L} \delta_{k,l-1}). \quad (59)$$

Let us consider that the nearly degenerate states $|\tilde{g}0\rangle$ and $|\tilde{e}, -n\rangle$ are coupled to each other through $v_{-n}^{\tilde{g}\tilde{e}}$ defined in

Eq. (52), where $-\varepsilon_0/2 \approx \varepsilon_0/2 - n\omega$. The infinite-dimensional matrix of H_F on the basis of $\{|\tilde{g}n\rangle, |\tilde{e}m\rangle\}$ is reduced to an effective 2×2 matrix within $|\tilde{g}0\rangle$ and $|\tilde{e}, -n\rangle$ using the Van Vleck perturbation theory. The perturbation parameters are $|\Delta|$ and $|A_T|$. Using a similar matrix form in Refs. 16 and 17, we present an effective Hamiltonian for $|\Delta|/\omega, |A_T|/\omega \ll 1$:

$$\tilde{H}_F = \begin{pmatrix} -\frac{\varepsilon_0}{2} + \delta & v_{-n}^{\tilde{g}\tilde{e}} \\ v_{-n}^{\tilde{e}\tilde{g}} & \frac{\varepsilon_0}{2} - \delta - n\omega \end{pmatrix}, \quad (60)$$

where δ is the energy shift that corresponds to the ac Stark shift,^{16,17)} and the off-diagonal matrix element is represented by the first order of the perturbation parameters as

$$\begin{aligned} v_k^{\tilde{g}\tilde{e}} &= \left(v_k^{\tilde{e}\tilde{g}}\right)^* \\ &= e^{-ik\theta_L} \left[\frac{\Delta^*}{2} J_k \left(\frac{|A_L|}{\omega}\right) + \frac{|A_T|}{4} e^{i(\theta_T - \theta_L)} J_{k+1} \left(\frac{|A_L|}{\omega}\right) \right. \\ &\quad \left. + \frac{|A_T|}{4} e^{-i(\theta_T - \theta_L)} J_{k-1} \left(\frac{|A_L|}{\omega}\right) \right]. \end{aligned} \quad (61)$$

The leading term of δ is given by

$$\delta = - \sum_{\substack{k=-\infty \\ k \neq -n}}^{\infty} \frac{|v_k^{\tilde{g}\tilde{e}}|^2}{\varepsilon_0 + k\omega}, \quad (62)$$

which indicates that an n -phonon resonance occurs at $\varepsilon_0 = n\omega + 2\delta$. Indeed, the eigenvalues of \tilde{H}_F are

$$q_{\pm} = -\frac{n\omega}{2} \pm \sqrt{\frac{(n\omega - \varepsilon_0 + 2\delta)^2}{4} + |v_{-n}^{\tilde{g}\tilde{e}}|^2}, \quad (63)$$

which lead to the time-dependent transition probability from $|g\rangle$ to $|e\rangle$ mediated by n phonons

$$P_{g \rightarrow e}^{(n)}(t) = \frac{|v_{-n}^{\tilde{g}\tilde{e}}|^2}{\tilde{q}^2} \sin^2 \tilde{q}t = \frac{|v_{-n}^{\tilde{g}\tilde{e}}|^2}{\tilde{q}^2} \frac{1 - \cos 2\tilde{q}t}{2}, \quad (64)$$

where $\tilde{q} = \sqrt{(n\omega - \varepsilon_0 + 2\delta)^2/4 + |v_{-n}^{\tilde{g}\tilde{e}}|^2}$. In the long-time limit, we obtain the n -phonon time-averaged transition probability

$$\bar{P}_{g \rightarrow e}^{(n)} = \frac{1}{2} \frac{|v_{-n}^{\tilde{g}\tilde{e}}|^2}{|v_{-n}^{\tilde{g}\tilde{e}}|^2 + (n\omega - \varepsilon_0 + 2\delta)^2/4}. \quad (65)$$

The broadening of the transition peaks $4|v_{-n}^{\tilde{g}\tilde{e}}|^2$ depends on the following model parameters

$$\Delta \equiv |\Delta|e^{i\phi_l}, \quad \theta_{TL} \equiv \theta_T - \theta_L, \quad J_k \equiv J_k \left(\frac{|A_L|}{\omega}\right), \quad (66)$$

and is explicitly written as

$$\begin{aligned} |v_{-n}^{\tilde{g}\tilde{e}}|^2 &= \frac{1}{4} \left\{ J_{-n}^2 \left(|\Delta| \cos \phi_l - n\omega \frac{|A_T|}{|A_L|} \cos \theta_{TL} \right)^2 \right. \\ &\quad \left. + \left[J_{-n} |\Delta| \sin \phi_l \right. \right. \\ &\quad \left. \left. - \frac{|A_T|}{2} (J_{-n+1} - J_{-n-1}) \sin \theta_{TL} \right]^2 \right\}. \end{aligned} \quad (67)$$

3. Results

First, the A_L and A_T dependence of the transition probability in the two-level system is investigated by solving Eqs. (42)–(44). When $|A_L|$ and $|A_T|$ are fixed, the transition

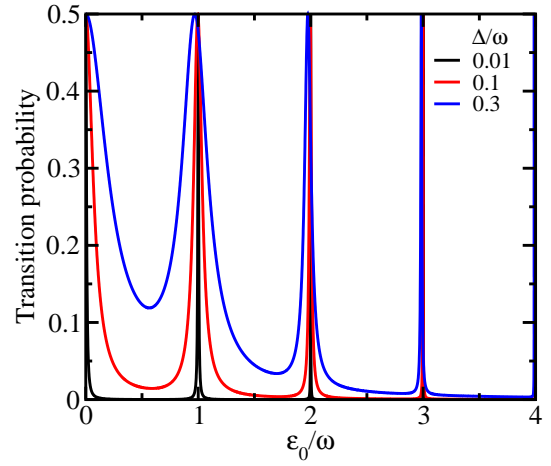


Fig. 3. (Color online) Transition probability for the L -mode phonons plotted as a function of the energy difference between the two states ε_0/ω for various values of the photon coupling Δ . Here, ω is the phonon energy that corresponds to the SAW frequency. $A_L/\omega = 1$ is chosen for the L -mode coupling and $A_T = 0$.

probability depends on the phase difference θ_{TL} between the L -mode and T -mode phonons. Although it is also dependent on the photon coupling represented by $|\Delta|e^{i\phi_l}$, the phase ϕ_l effect on the transition probability is negligibly small for $|\Delta|/\omega \ll 1$, where ω is the energy of a single phonon.

Next, the roles of QS couplings in the transition probability are elucidated for the two basis states split by a magnetic field and coupled to each other through the quadrupole operators in Eqs. (25) and (26). As described in Sect. 2.2, ω_0 corresponds to the Zeeman energy of the level splitting. The QS couplings A_L and A_T in Eq. (10) depend on the rotation angle θ of the magnetic field. Both couplings are determined from the combination of the three strain modes in Eq. (29). For a quartet system such as the Γ_8 state in the silicon vacancy, we have assumed that the magnetic field is strong enough ($\varepsilon_0/\omega \sim 1$) to neglect the contribution from the higher excited states, namely, the O_v coupling between the ground and second excited states. Although we focus on a single phonon process near $\varepsilon_0/\omega = 1$, we show the results for the two-level system including the $\varepsilon_0/\omega \ll 1$ parameter region to elucidate the roles of longitudinal and transverse QS couplings in the field-dependent transition probability. Indeed, inclusion of the higher excited states in the present model is required for a quantitative analysis of the quartet case, especially for a small magnetic field.

3.1 Effects of longitudinal and transverse phonon couplings on time-averaged transition probability

Let us consider the L -mode for $A_T = 0$ at first. The detailed study was already reported by a similar model used for the multiphoton quantum interference.¹⁶⁾ Here, the role of photons is replaced by that of L -mode phonons, while the photon is involved in the transition probability at $\varepsilon_0 = 0$ if there is no contribution from the phonons. For $A_L = 0$, the transition probability shows the maximum $1/2$ only at $\varepsilon_0 = 0$ that corresponds to a low magnetic field $H_z \sim \omega_l \ll \omega$. On the other hand, in the absence of the photon coupling ($\Delta = 0$), the transition cannot be caused by the L -mode phonons for $A_L \neq 0$. Thus, the photon-assisted process is

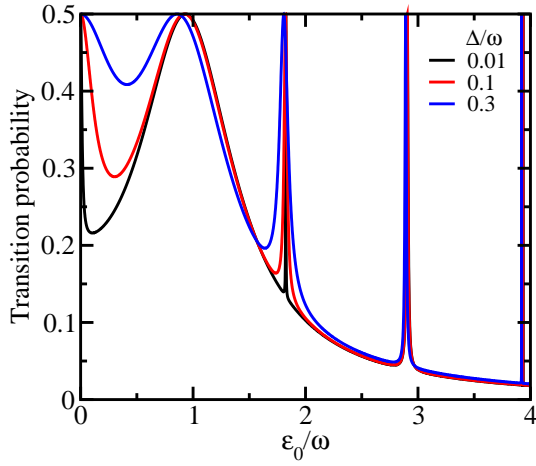


Fig. 4. (Color online) Transition probability for the T -mode phonons plotted as a function of ε_0/ω for various Δ , where $A_T/\omega = 1$ is chosen for the T -mode coupling and $A_L = 0$.

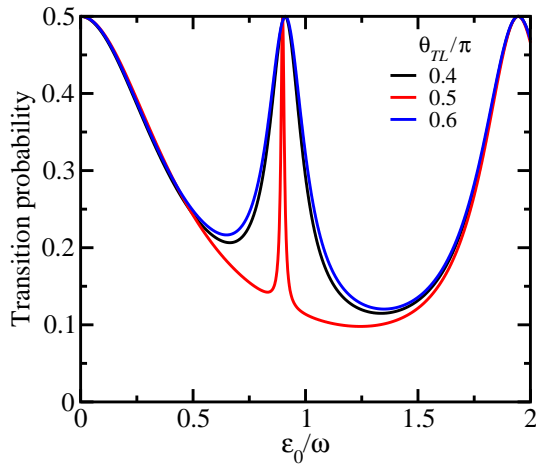


Fig. 5. (Color online) Transition probability for the two-level system coupled to both L -mode and T -mode phonons plotted as a function of ε_0/ω for $\Delta/\omega = 0.01$. The amplitudes of the L -mode ($A_L = |A_L|e^{i\theta_L}$) and T -mode ($A_T = |A_T|e^{i\theta_T}$) couplings are fixed as $|A_L|/\omega = 1.8$ and $|A_T|/\omega = 0.8$. The broadness of the peak near $\varepsilon_0/\omega = 1$ is sensitively dependent on the phase difference of the two modes $\theta_{TL} = \theta_T - \theta_L$ around $\theta_{TL}/\pi = 0.5$.

required for a finite transition probability coupled to the L -mode phonons, and the transition probability peaks reach $1/2$ at nearly $\varepsilon_0 = \omega, 2\omega, \dots$. This indicates a possibility of MAR with the use of the L -mode phonons. Figure 3 shows that the transition probability peaks become sharp at $\varepsilon_0 = n\omega$ for $|\Delta|/\omega \ll 1$. As $|\Delta|$ increases, each peak broadens and the n th peak position ε_0 shifts towards a lower value from $\varepsilon_0 = n\omega$. In particular, the single phonon process at $\varepsilon_0 = \omega$ shows the largest shift. This result is inferred from Eqs. (62), (65) and (67). The broadness of the peaks are represented approximately by $4|v_{-n}^{\tilde{e}}| \approx 2|\Delta|J_n(|A_L|/\omega)$ and the peak shifts also obey $|v_{k\pm n}^{\tilde{e}}|^2$ for $|\Delta|/\omega \ll 1$. The calculated transition probability for $A_T = 0$ does not depend on the phase shifts ϕ_l and θ_L .

Next, we show the role of the T -mode phonon in the absence of the L -mode for $A_L = 0$. This was originally investigated by Shirley, formulating the Floquet theory for the two-level system with an oscillating field, and corresponds to

$\Delta \rightarrow 0$ in our model.¹⁵⁾ In particular, for $|A_T|/\omega \lesssim 1$, the transition probability shows narrow peaks near $\varepsilon_0 = 3\omega, 5\omega, \dots$ and a relatively broad peak near $\varepsilon_0 = \omega$. When $|\Delta|$ is finite, additional narrow peaks emerge near $\varepsilon_0 = 2\omega, 4\omega, \dots$ and the peak widths become broader with increasing $|\Delta|$ as shown in Fig. 4. For a relatively large $|\Delta|$, the peak at $\varepsilon_0 \approx \omega$ merges into the peak at $\varepsilon_0 = 0$, and the transition probability shows an almost constant value close to $1/2$ in $0 < \varepsilon_0 < \omega$. This indicates that the contribution from the higher excited states may not be negligible in the quartet case discussed in Sect. 2.2.

To elucidate the roles of the phonon coupling with the L - and T -modes together in the transition probability, we devote ourselves to a small $|\Delta|/\omega < 0.1$ for the photon coupling, where the effect of the photon phase shift ϕ_l is negligible. When both A_L and A_T are finite, the phase difference θ_{TL} of the two phonon modes affects the transition probability to some extent. This is an important point for the MAR assisted by photons. Here, we examine a single phonon resonance for $|A_T|/|A_L| < 1$ to show explicitly a key role of a finite A_T . The A_T effect brings about the broadness of a narrow peak in the transition probability at $\varepsilon_0 = \omega$ and also shifts the peak position ε_0 towards a lower value from ω . It is specially marked that the sharpness of the peak becomes prominent for $|A_L|/\omega \approx 1.8$. This is explained by Eq. (67) in which the difference of the Bessel functions ($J_0 - J_2$) almost vanishes for $n = 1$. In addition, the resonance peak becomes narrower when θ_{TL} is adjusted to satisfy $\cos \theta_{TL} = (|\Delta||A_L|)/(\omega|A_T|) \approx 1.8|\Delta|/|A_T| < 1$, where $|v_{-1}^{\tilde{e}}|$ is almost close to zero. The θ_{TL} dependence is shown for $\Delta/\omega = 0.01$, $|A_L|/\omega = 1.8$ and $|A_T|/\omega = 0.8$ in Fig. 5. According to Eq. (29), the QS couplings depend on the rotation angle θ of the magnetic field. Thus, $A_L = -g_L a_L e^{i\phi_L}$ and $A_T = g_T a_T e^{i\phi_T}$ can be controlled by the field angle for the appearance of such a sharp transition probability peak as demonstrated in the next subsection.

3.2 Effects of quadrupole-strain couplings on time-averaged transition probability

On the basis of the QS couplings described by Eqs. (28)–(34), we change the quadrupole coupling constants (g_{Γ_3} and g_{Γ_5}), the local strain amplitudes (a_U , a_V , and a_{ZX}) and the relative time-independent phase shifts of the SAW modes (ϕ_U and ϕ_V measured from $\phi_{ZX} = 0$). Here, $a_U = a_V$ is set for simplicity, so that the weight of the Γ_3 and Γ_5 QS couplings in the two-level system is represented by the ratio of $g_{\Gamma_3} a_U$ and $g_{\Gamma_5} a_{ZX}$. The energy difference between the two states is changed as $\varepsilon_0 \propto H_z$ and the z axis of the field orientation is rotated as $(\sin \theta, 0, \cos \theta)$ in the ZX plane of the crystal (see Fig. 2). First, we compute $|A_L|$, $|A_T|$ and θ_{TL} as a function of the field angle θ for given $g_{\Gamma_3} a_U$, $g_{\Gamma_5} a_{ZX}$, ϕ_U , and ϕ_V . Next, we solve the eigenvalue problem of H_F in Eq. (44) to obtain the time-averaged transition probability in Eq. (45) as a function of θ for the fixed $\varepsilon_0 = \omega$ and as a function of ε_0 for various values of θ . In the following, a single phonon process is intensively studied to elucidate a new aspect of the quadrupoles.

Figure 6 (a) shows a Γ_5 -component dominant case ($g_{\Gamma_5} a_{ZX} > g_{\Gamma_3} a_U$), choosing $\phi_U = \phi_V = \phi_{ZX} = 0$ and fixing the two-level splitting at $\varepsilon_0 = \omega$. The transition probability is plotted as a function of the field angle θ , and it shows very narrow dips at $\theta \approx \pm\pi/4$. In Eq. (29), $|A_T| = g_T a_T \approx |C_{T,1} \cos 2\theta|$ owing to $|C_{T,1}| \gg |C_{T,2}|$, and $|A_T|$ almost vanishes at $\theta \approx \pm\pi/4$, namely, $|A_T| \ll |A_L| = g_L a_L$. Both $g_L a_L$ and $g_T a_T$ are also

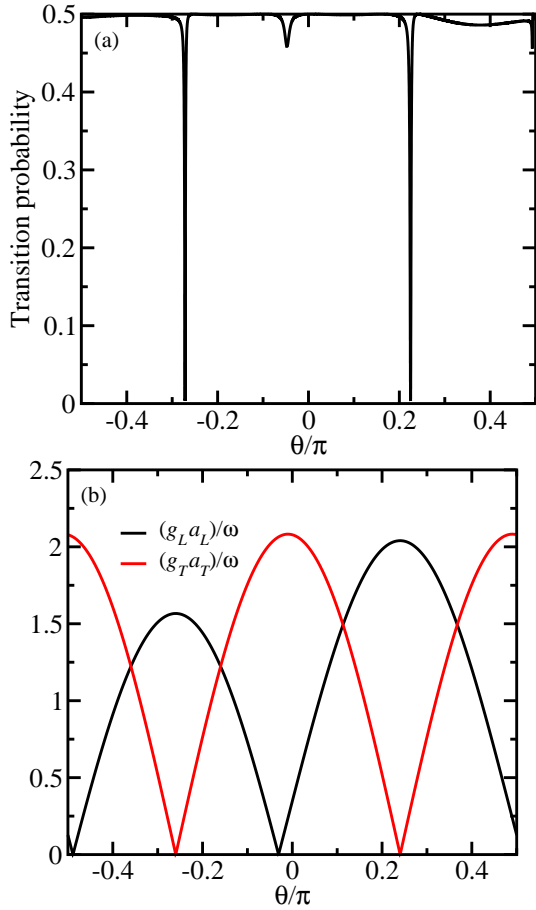


Fig. 6. (Color online) (a) Transition probability $P_{\epsilon_0=\omega}$ at $\epsilon_0/\omega = 1$ plotted as a function of the magnetic-field angle θ for $\Delta/\omega = 0.1$. (b) L -mode ($g_L a_L$) and T -mode ($g_T a_T$) QS couplings plotted as a function of θ . The data are plotted for $(g_{\Gamma_3} a_U)/\omega = 0.1$, $(g_{\Gamma_5} a_{ZX})/\omega = 0.6$, and $\phi_U = \phi_V = \phi_{ZX} = 0$.

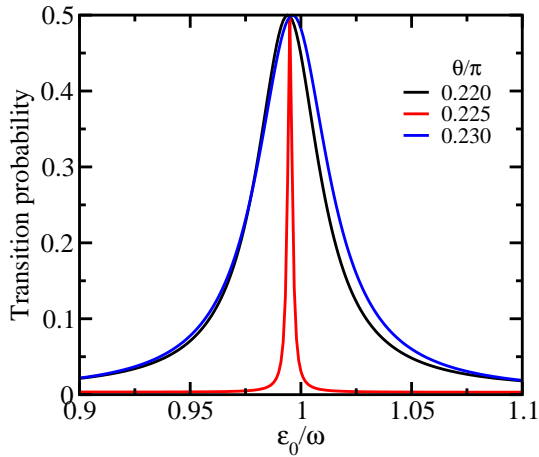


Fig. 7. (Color online) Transition probability for single phonon process. The data are plotted as a function of ϵ_0/ω for various values of θ near $\theta/\pi = 0.225$ at which $P_{\epsilon_0=\omega}$ shows the narrow dip in Fig. 6.

plotted as a function of θ in Fig. 6 (b) and indicates that the L -mode coupling is dominant at $\theta \simeq \pm\pi/4$. The origin of the dips is explained by the appearance of a sharp transition probability peak as shown in Fig. 7. Notice that the energy of the peak position shifts towards a lower value from $\epsilon_0 = \omega$. When θ is

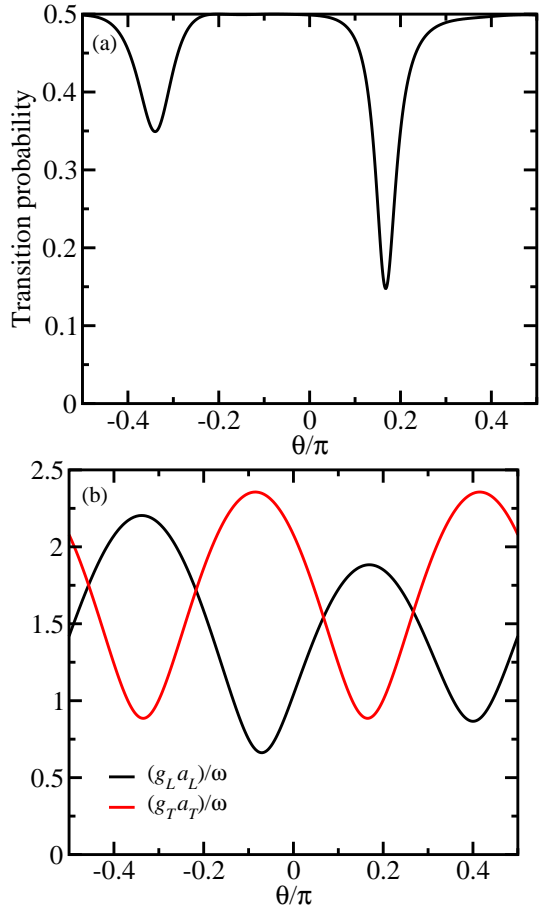


Fig. 8. (Color online) (a) Transition probability $P_{\epsilon_0=\omega}$ at $\epsilon_0/\omega = 1$ plotted as a function of the magnetic-field angle θ for $\Delta/\omega = 0.01$. (b) L -mode ($g_L a_L$) and T -mode ($g_T a_T$) QS couplings plotted as a function of θ . The data are plotted for $(g_{\Gamma_3} a_U)/\omega = 0.3$, $(g_{\Gamma_5} a_{ZX})/\omega = 0.6$, and the phase shifts of the three SAW strain modes are chosen as $\phi_U/\pi = 0.25$, $\phi_V/\pi = -0.75$, and $\phi_{ZX} = 0$.

varied from the above value for the sharp peak ($\theta/\pi = 0.225$ in Fig. 7), the peak broadening causes the abrupt increase in the θ -dependent transition probability $P_{\epsilon_0=\omega}$ at $\epsilon_0 = \omega$ in Fig. 6 (a). This is a key to the microscopic measurement of the quadrupole components. The L -mode-phonon-mediated transition is always accompanied by the photon absorption, and the corresponding resonance can be detected by the EPR measurement. For the same phase shifts $\phi_U = \phi_V = \phi_{ZX}$, the narrow dips in the θ -dependent $P_{\epsilon_0=\omega}$ become invisible as the photon coupling $|\Delta|$ decreases. It is because the resonance peak appears exactly at $\epsilon_0 = \omega$. Instead, the similar narrow dips can be found when ϵ_0 is slightly shifted from ω (for instance, $\epsilon_0/\omega = 1.01$).

In generic, the difference of phase shifts ϕ_U , ϕ_V , and ϕ_{ZX} ($= 0$) has to be considered for the θ dependence of the transition probability, which can be controlled by the SAW experiment. Here, we show the data for $|\phi_U - \phi_V| = \pi$ taking account of the phase difference between two strains ϵ_U and ϵ_V reported by the previous SAW experiment of the silicon wafer.¹¹⁾ The photon coupling is fixed at $\Delta = 0.01$, which is small enough to treat Δ as a real number. In Fig. 8 (a), the two dips are also found in the θ -dependent $P_{\epsilon_0=\omega}$. Since $(g_{\Gamma_5} a_{ZX})/(g_{\Gamma_3} a_U) > 1$, the field angle θ for the minimum transition probability slightly shifts towards a lower value from

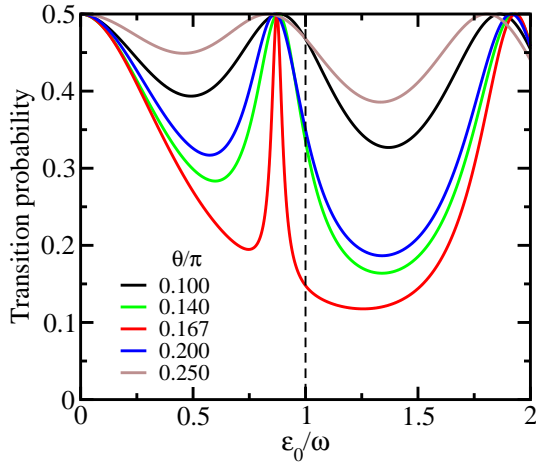


Fig. 9. (Color online) Transition probability plotted as a function of ε_0/ω for various θ around $\theta/\pi = 0.167$ for the minimum $P_{\varepsilon_0=\omega}$ in Fig. 8.

$\pi/4$. This is also explained by the existence of a sharp transition probability peak at a lower value of ε_0 shifted from ω as shown in Fig. 9. The resonance near $\varepsilon_0 = \omega$ is owing to the L -mode dominant contribution. In Fig. 8 (b), $|A_L| (= g_L a_L)$ almost reaches a local maximum ($\approx 1.8\omega$) when $|A_T| (= g_T a_T)$ equals a local minimum. Let us consider the field angle θ_{dip} for the minimum $P_{\varepsilon_0=\omega}$. This θ_{dip} almost equals the value for the minimum $|A_T|$, which can be evaluated by Eq. (29). Using $\xi \equiv (g_{\Gamma_3} a_U)/(g_{\Gamma_5} a_{ZX})$, $|A_T|$ is rewritten as

$$\frac{|A_T|^2}{6(g_{\Gamma_5} a_{ZX})^2} = 1 + \xi^2 \left(1 + \frac{\sqrt{3}}{2} \right) + A_{\phi_U} \cos(4\theta + \alpha), \quad (68)$$

and

$$A_{\phi_U}^2 = \left[1 - \xi^2 \left(1 + \frac{\sqrt{3}}{2} \right) \right]^2 + \xi^2 (1 + \sqrt{3})^2 \cos^2 \phi_U, \quad (69)$$

$$\tan \alpha = \frac{\xi(1 + \sqrt{3})}{1 - \xi^2 \left(1 + \frac{\sqrt{3}}{2} \right)} \cos \phi_U. \quad (70)$$

When the Γ_5 component is dominant as $\xi \ll 1$ and $A_{\phi_U} > 0$, one of the conditions for the minimum $|A_T|$ is given by $\theta = (\pi - |\alpha|)/4$ for $0 < |\phi_U| < \pi/2$. This equation also indicates that for $\pi/2 < |\phi_U| < \pi$, the transition probability shows a similar dip near the negative $\theta = -(\pi - |\alpha|)/4$. On the other hand, for $\xi \gg 1$ and $A_{\phi_U} < 0$ which correspond to the Γ_3 -dominant case, one can find that these values θ are replaced by $|\alpha|/4$ and $-|\alpha|/4$, respectively. When θ differs from θ_{dip} in Fig. 9, the transition probability peak broadens keeping the peak position ε_0 at almost the same value. This broadening comes from the T -mode contribution. In the quartet case discussed in Sect. 2.2, the contribution from the higher excited states may not be negligible when the peak at $\varepsilon_0/\omega \approx 1$ merges into the peak at $\varepsilon_0 = 0$ for $\theta/\pi \approx 0.1$ or $\theta/\pi \approx 0.25$.

We conclude that it is essential to find the field angle θ_{dip} for the sharp resonance peak. Owing to the photon-assisted transition dominated by the L -mode phonon, the resonance peak can be probed by the EPR measurement. This θ_{dip} is related to the ratio ξ of the QS couplings with the different symmetries Γ_3 and Γ_5 . In addition, the ratio of the quadrupole coupling constants g_{Γ_3} and g_{Γ_5} can be evaluated from the measurement

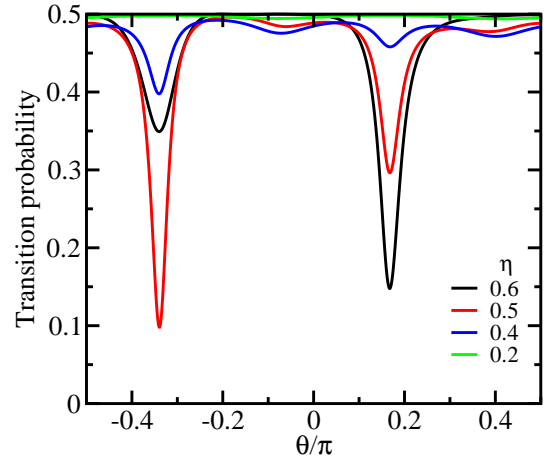


Fig. 10. (Color online) Transition probability $P_{\varepsilon_0=\omega}$ at $\varepsilon_0/\omega = 1$ plotted as a function of the magnetic-field angle θ . The phase shifts of the three SAW strain modes are chosen as $\phi_U/\pi = 0.25$, $\phi_V/\pi = -0.75$, and $\phi_{ZX} = 0$. Here, $g_{\Gamma_3} a_U = g_{\Gamma_3} a_V = 0.5g_{\Gamma_5} a_{ZX}$, and the data are plotted for various values of $\eta \equiv (g_{\Gamma_5} a_{ZX})/\omega \leq 0.6$. The data for $\eta = 0.6$ is the same as $P_{\varepsilon_0=\omega}$ in Fig. 8.

of the local strain amplitudes a_i ($i = U, V, ZX$).

Owing to the penetration of the SAW into the solid, the strain amplitudes a_i show the same exponential decay along the Z axis¹¹⁾ and cause a significant decrease in $|A_L|$ and $|A_T|$. Since the ratio of $g_{\Gamma_3} a_U$, $g_{\Gamma_3} a_V$, and $g_{\Gamma_5} a_{ZX}$ is unchanged, $|A_T|/|A_L|$ keeps the θ dependence obtained on the surface ($Z = 0$) during the decay of a_i . Accordingly, the local minimums of $P_{\varepsilon_0=\omega}$ appear at almost the same values θ as shown in Fig. 10, where η is defined as the value of $(g_{\Gamma_5} a_{ZX})/\omega$ keeping $g_{\Gamma_3} a_U = g_{\Gamma_3} a_V = 0.5g_{\Gamma_5} a_{ZX}$. The origin of the left narrow dip at $\theta/\pi = -0.340$ for $\eta = 0.5$ is also explained by the local maximum $|A_L| = g_L a_L \approx 1.8\omega$. This is evaluated from the value of $(5/6)g_L a_L$ in Fig. 8 (b) plotted for $\eta = 0.6$. For small a_i ($\eta < 0.2$), $P_{\varepsilon_0=\omega}$ shows almost constant values $\approx 1/2$ in the entire region $-\pi/2 \leq \theta \leq \pi/2$. Thus, the decay of a_i does not affect the appearance of the dips in the θ -dependent transition probability. In the single phonon process at $\varepsilon_0 \approx \omega$, $|A_L|/\omega \approx 1.8$ is the most appropriate condition for detecting the photon-assisted L -mode phonon resonance, which is explained by Eq. (67) as discussed in Sect. 3.1. This condition of $|A_L|$ can be accessed by tuning the frequency ω and the amplitudes a_i of the SAW strain modes.

4. Conclusion and Discussion

In this paper, we have studied a minimum model of the two-level system for the hybrid EPR-MAR measurement and have demonstrated how the dynamical QS couplings can be evaluated by the magnetic field angle dependence of the time-averaged transition probability. Here, the photon frequency is negligibly small compared to the phonon frequency of gigahertz order. The longitudinal (L -mode, A_L) and transverse (T -mode, A_T) couplings of the two states are related to the three phonon modes of elastic strains (ε_U , ε_V , and ε_{ZX}). These are driven by the SAW propagating in the principal axis (X axis). The key point is that both couplings are changed by rotating the magnetic field since the combination of the three QS couplings depends on the rotation angle.

Using the Floquet theory, we have investigated the effects of L -mode and T -mode couplings on the transition probability

as a function of ε_0/ω , where ε_0 and ω are the energy difference of the two states and the SAW phonon frequency, respectively. It is essential to focus on the single phonon process for $\varepsilon_0/\omega \lesssim 1$. The sharpness of the transition probability peak originates from the L -mode coupling effect assisted by the phonon with a small coupling Δ , while the peak broadening at $\varepsilon_0/\omega \approx 1$ is owing to the T -mode coupling. The appearance of the transition probability peaks also depends on the phase difference between the L -mode and T -mode couplings.

On the basis of this result, we have shown the effects of the QS couplings on the transition probability at $\varepsilon_0/\omega = 1$ as a function of the field angle θ for a Γ_5 -quadrupole dominant case. The important finding is the appearance of the two narrow dips in the transition probability owing to the vanishment of $|A_T|$ and the approach of $|A_L|$ to a local maximum. The origin of the dips is explained by the lower energy shift of a sharp resonance peak from $\varepsilon_0/\omega = 1$ and the strong θ dependence of the peak broadening. Experimentally, the field angle for the sharp resonance can be probed by the EPR measurement since the photon-assisted transition becomes more significant for $|A_L| > |A_T|$. This is important for evaluating the ratio of QS couplings with different symmetries.

In the hybrid EPR-MAR measurement as described above, the L -mode phonon plays an important role in the appearance of a sharp resonance peak in the field-angle-dependent transition probability. Since the L -mode coupling is usually inactive in the transition process, we have introduced the idea of photon-assisted MAR and demonstrated how to extract a dominant L mode for the MAR from the various phonon modes. The sharpness of the resonance peak becomes more prominent for a weak photon field, which may allow high sensitivity in the conventional optical measurements.

For the silicon vacancy presented in Sect. 2.2, the ratio of the Γ_3 and Γ_5 QS coupling constants $g_{\Gamma_5}/g_{\Gamma_3} = 1.6$ was reported by the low-temperature ultrasonic measurement.⁹⁾ This indicates the Γ_5 -quadrupole dominant case as discussed in Sect. 3.2 when the amplitudes of elastic strains are almost the same in magnitude. It is expected that the field angle for a sharp resonance appears in $1/8 < \theta/\pi < 1/4$. Indeed, the θ -dependent transition probability also depends on the phase differences between the strain modes driven by the SAW. Thus, the evaluation of the QS coupling constants requires precise measurement of a_i and ϕ_i of the strains represented by $\varepsilon_i = a_i \cos(\omega t + \phi_i)$ ($i = U, V, ZX$).

The idea of the hybrid EPR-MAR measurement can also be applied to reveal hidden quadrupole properties in the $S = 1$ ground state of the NV center. For the NV spin state in the C_{3v} crystal-field environment, electronic dipoles belong to the same point-group character as electric quadrupoles represented by the second-rank spin tensors:^{2,22-24)} $Q_x = S_x^2 - S_y^2$ and $Q_{zx} = S_z S_x + S_x S_z$ for the x component of the dipole; $Q_{xy} = S_x S_y + S_y S_x$ and $Q_{yz} = S_y S_z + S_z S_y$ for the y component. Among them, there has been a lack of information on the relevance of Q_{zx} and Q_{yz} to electric-field control of the NV spin.^{23,25)} A possibly significant role of these quadrupoles has been pointed out by the recent theoretical proposal of mechanically and electrically driven electron spin resonance as a new application of spin-strain interactions in the NV center.²⁾ More detailed investigations of the unknown quadrupole couplings are required to realize a promising platform of spin-controlled devices for quantum information processing and

sensing applications.²⁶⁾

It will be also intriguing to apply our idea to revisit various quadrupole properties in well-localized f -electron systems such as CeB₆.^{7,27)} It is expected that the antiferroquadrupole ordering transition in CeB₆ affects the local f -electron level structure with the Γ_8 symmetry, which can modify a photon-phonon coupling process in the EPR measurement under a propagating SAW of gigahertz order. According to the resonant x-ray diffraction experiment, a linear combination of quadrupole order parameters is continuously changed by controlling the direction of an applied magnetic field.²⁸⁾ This is a new aspect of quadrupole dynamics that is detectable in various orbitally degenerate electron systems.

This work was supported by JSPS KAKENHI Grant Number 17K05516.

- 1) Y. Okazaki, I. Mahboob, K. Onomitsu, S. Sasaki, S. Nakamura, N. Kaneko, and H. Yamaguchi, Nat. Commun. **9**, 2993 (2018).
- 2) P. Udvarhelyi, V. O. Shkolnikov, A. Gali, G. Burkard, and A. Pályi, Phys. Rev. B **98**, 075201 (2018).
- 3) D. A. Golter, T. Oo, M. Amezcua, K. A. Stewart, and H. Wang, Phys. Rev. Lett. **116**, 143602 (2016).
- 4) D. A. Golter, T. Oo, M. Amezcua, I. Lekavicius, K. A. Stewart, and H. Wang, Phys. Rev. X **6**, 041060 (2016).
- 5) H. Y. Chen, E. R. MacQuarrie, and G. D. Fuchs, Phys. Rev. Lett. **120**, 167401 (2018).
- 6) The recent experiment of SAW coupled to magnetic resonance has been reported by R. Sasaki, Y. Nii, and Y. Onose, Phys. Rev. B **99**, 014418 (2019).
- 7) Y. Kuramoto, H. Kusunose, and A. Kiss, J. Phys. Soc. Jpn. **78**, 072001 (2009).
- 8) T. Goto, H. Yamada-Kaneta, Y. Saito, Y. Nemoto, K. Sato, K. Kakimoto, and S. Nakamura, J. Phys. Soc. Jpn. **75**, 044602 (2006).
- 9) S. Baba, M. Akatsu, K. Mitsumoto, S. Komatsu, K. Horie, Y. Nemoto, H. Yamada-Kaneta, and T. Goto, J. Phys. Soc. Jpn. **82**, 084604 (2013).
- 10) K. Okabe, M. Akatsu, S. Baba, K. Mitsumoto, Y. Nemoto, H. Yamada-Kaneta, T. Goto, H. Saito, K. Kashima, and Y. Saito, J. Phys. Soc. Jpn. **82**, 124604 (2013).
- 11) K. Mitsumoto, M. Akatsu, S. Baba, R. Takasu, Y. Nemoto, T. Goto, H. Yamada-Kaneta, Y. Furumura, H. Saito, K. Kashima, and Y. Saito, J. Phys. Soc. Jpn. **83**, 034702 (2014).
- 12) H. Matsuura and K. Miyake, J. Phys. Soc. Jpn. **77**, 043601 (2008).
- 13) T. Yamada, Y. Yamakawa, and Y. Ōno, J. Phys. Soc. Jpn. **78**, 054702 (2009).
- 14) T. Ogawa, K. Tsuruta, H. Iyetomi, Solid State Commun. **151**, 1605 (2011).
- 15) J. H. Shirley, Phys. Rev. **138**, B979 (1965).
- 16) S.-K. Son, S. Han, and S.-I. Chu, Phys. Rev. A **79**, 032301 (2009).
- 17) J. Hausinger and M. Grifoni, Phys. Rev. A **81**, 022117 (2010).
- 18) A. Eckardt and E. Anisimovas, New J. Phys. **17**, 093039 (2015).
- 19) T. Mikami, S. Kitamura, K. Yasuda, N. Tsuji, T. Oka, and H. Aoki, Phys. Rev. B **93**, 144307 (2016) [Errata **99**, 019902(E) (2019)].
- 20) S.-I. Chu and D. A. Telnov, Phys. Rep. **390**, 1 (2004).
- 21) T. Nakai, Bull. Nucl. Magn. Resonance Soc. Jpn. **7**, 33 (2016) [in Japanese].
- 22) E. Van Oort and M. Glasbeek, Chem. Phys. Lett. **168**, 529 (1990).
- 23) M. W. Doherty, F. Dolde, H. Fedder, F. Jelezko, J. Wrachtrup, N. B. Manson, and L. C. L. Hollenberg, Phys. Rev. B **85**, 205203 (2012).
- 24) M. Matsumoto, K. Chimata, and M. Koga, J. Phys. Soc. Jpn. **86**, 034704 (2017).
- 25) M. W. Doherty, N. B. Manson, P. Delaney, F. Jelezko, J. Wrachtrup, and L. C. L. Hollenberg, Phys. Rep. **528**, 1 (2013).
- 26) D. Suter and F. Jelezko, Prog. Nucl. Magn. Resonance Spectrosc. **98-99**, 50 (2017).
- 27) R. Shiina, H. Shiba, and P. Thalmeier, J. Phys. Soc. Jpn. **66**, 1741 (1997).
- 28) T. Matsumura, T. Yonemura, K. Kunitani, M. Sera, F. Iga, T. Nagao, and J. Igarashi, Phys. Rev. B **85**, 174417 (2012).